Synchronization and fluctuations: Coupling a finite number of stochastic units

Alexandre Rosas,[1] Jaime Cisternas,[2] Daniel Escaff,[2] Italo'Ivo Lima Dias Pinto,[3] and Katja Lindenberg[4]
[1]*Departamento de Física, CCEN, Universidade Federal da Paraíba, Caixa Postal 5008, 58059-900, João Pessoa, Brazil*
[2]*Complex Systems Group, Facultad de Ingeniería y Ciencias Aplicadas, Universidad de los Andes, Santiago, Chile*
[3]*Physics Department, Federal University of Pernambuco (UFPE), Recife, PE 50670-901, Brazil*
[4]*Department of Chemistry and Biochemistry and BioCircuits Institute, University of California San Diego, La Jolla, California 92093-0340, USA*

(Received 14 October 2019; revised manuscript received 2 March 2020; accepted 23 April 2020; published 25 June 2020)

It is well established that ensembles of globally coupled stochastic oscillators may exhibit a nonequilibrium phase transition to synchronization in the thermodynamic limit (infinite number of elements). In fact, since the early work of Kuramoto, mean-field theory has been used to analyze this transition. In contrast, work that directly deals with finite arrays is relatively scarce in the context of synchronization. And yet it is worth noting that finite-number effects should be seriously taken into account since, in general, the limits $N \to \infty$ (where N is the number of units) and $t \to \infty$ (where t is time) do not commute. Mean-field theory implements the particular choice first $N \to \infty$ and then $t \to \infty$. Here we analyze an ensemble of three-state coupled stochastic units, which has been widely studied in the thermodynamic limit. We formally address the finite-N problem by deducing a Fokker-Planck equation that describes the system. We compute the steady-state solution of this Fokker-Planck equation (that is, finite N but $t \to \infty$). We use this steady state to analyze the synchronic properties of the system in the framework of the different order parameters that have been proposed in the literature to study nonequilibrium transitions.

DOI: 10.1103/PhysRevE.101.062140

I. INTRODUCTION

Systems consisting of many elements, when they are kept out of equilibrium, have the fascinating ability to exhibit collective coordinated behavior. The macroscopic variables that describe the system are no longer static and may display a complex spatiotemporal structure. Restricting our discussion to temporal structuring, since the pioneering work of Winfree [1] and Kuramoto [2] synchronization phenomena have become a paradigm of these sorts of self-organized behaviors [3–5].

Most of the work that addresses the synchronization problem focuses mainly on two types of systems: (1) a few identical deterministic oscillators that reach synchronization and (2) oscillators that include some degree of stochasticity (such as randomly distributed frequencies in the Kuramoto model, or internal noise in the oscillatory units) and study when synchronization is reached in the thermodynamic limit (infinite number N of elements). The first approach is mostly a dynamical systems problem, while the second has more ingredients of nonequilibrium statistical physics.

Here we focus on coupled stochastic units. Each unit is a three-state element where transitions between these states are governed by transition probabilities. This model has been used to study the synchronization problem in the thermodynamic limit $N \to \infty$ [6–11], analytically when the coupling among units is global (all-to-all interactions) using mean-field theory and numerically when the coupling is local (e.g., nearest-neighbor interactions), where the system exhibits a very interesting equilibrium-like critical behavior. In this paper, in contrast, we formally address the problem of a finite number of globally coupled identical units. We note that we use the term "synchronization" to describe the coherent motion of most units together from one state to the next and the next and back to the original state. In other words, we refer to periodic oscillations of the entire ensemble of elements.

It is worth noting that discrete state stochastic oscillator models that undergo a phase transition to synchronization or ordered behavior are frequently found in the literature. We mention just a few here. Insofar as these models are studied analytically, they all assume global coupling in the mean-field limit. In Ref. [12], globally coupled three-state oscillators are considered as a model of stochastic excitable systems. The authors consider a form of coupling that leads to a stable stationary state and another that exhibits coherent oscillations. In Ref. [13], still focusing on three-state stochastic oscillators, this work is extended to a broader class of non-Markovian systems, and the resultant collective oscillations are shown to occur in large parameter regimes. Ensembles of excitable stochastic two-state oscillators with delayed feedback are studied in Ref. [14] as an abstract representation of an excitable system. Here again, depending on the properties of the single oscillators and of the global coupling of an infinite number of them, the system exhibits bistability in some cases and bulk oscillations in others. Tsimring and coworkers [15,16] have an extensive bibliography on two-state and on three-state systems of coupled stochastic oscillators that undergo a variety of interesting transitions in the mean-field limit (too many to list here). Tsimring's work has now moved on to the construction of genetic regulatory circuits based on these

ideas, see, e.g., Ref. [17]. Our own work on coupled three-state stochastic oscillators [6–9] has been extended in interesting ways by Assis *et al.* [10,11], including the discovery of a symmetry-breaking transition to a steady state that has no counterpart in equilibrium statistical mechanics. Finally, we mention our work on two-state stochastic oscillators [18,19] where, still in the framework of mean-field theory, we studied the effect of a state-dependent memory on the synchronization process.

We have recently addressed the problem of a finite number of elements in the context of Markovian two-state units [20,21]. In this case, the fluctuations induced by the finite number of elements have an interesting multiplicative structure that can induce new features not predictable from mean-field theory. In other words, the limits $N \to \infty$ (where N is the number of elements) and $t \to \infty$ (where t is time) do not commute. To observe even more complex and permanent dynamics, we here go beyond two-state Markovian models. Three-state Markovian units constitute a good scenario to analyze synchronous oscillations that do not occur in two-state Markovian units.

The aim of this work is to formally treat the problem of fluctuations induced by finite numbers of elements in the context of synchronous oscillations based on a three-state stochastic unit as the fundamental constituent of our ensemble and thus to generalize our previous results for two-state elements [20,21]. It is worth noting that we have found the literature on finite arrays of phase-coupled oscillators of any kind that undergo phase transitions in the thermodynamic limit to be scarce. In fact, the only references we have identified deal with continuous-phase oscillators such as the extensively studied Kuramoto model. Even here finite arrays are still considered to be a relatively open problem [4,22,23].

We have organized this paper as follows. In Sec. II we present the model as well as summarize our earlier predictions in the framework of mean-field theory. We also present the microscopic equation that describes the dynamics of our array of N oscillators and show some numerical simulations of these microscopic dynamics. We discuss how the mean-field approach describes what we observe from direct numerical simulations. In Sec. III we present our formal theory for finite N. We obtain a Fokker-Planck equation for the ensemble which we can deduce in two different ways. One is to write a mesoscopic master equation for the array, from which, via an expansion in powers of $1/N$, we obtain the Fokker-Planck equation. The other is to directly start from the microscopic dynamics, from which we are able to deduce a set of Langevin equations that, in the framework of Itô calculus, lead to the same Fokker-Planck equation. We then compute the Fokker-Planck steady state by using a finite-element method and use this result to analyze the finite-N system in terms of different order parameters that have been proposed in the literature. Finally, in Sec. IV we present our conclusions and final remarks.

II. MODEL AND MEAN-FIELD THEORY

In this section we present the model to be analyzed. First we summarize the known results in the framework of mean-field theory.

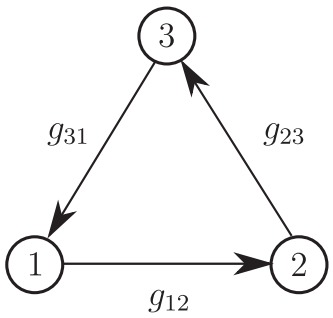

FIG. 1. Representation of the three possible states of a unit and the allowed stochastic transitions.

A. Single unit dynamics

Our starting point is an oscillator that can be in one of three states, say, $\{1, 2, 3\}$. For a single oscillator, transitions between these states are stochastic and governed by the rates g_{ij}, that is, the probability to undergo a transition from state i to state j at any time within the interval $[t, t + dt]$ has the form

$$\mathbb{P}(i \to j, \{t, dt\}) = g_{ij}dt + \mathcal{O}(dt^2). \tag{1}$$

Thus, the model is Markovian, and the stochastic dynamics are dictated by an exponential distribution of the residence times in each state. Furthermore, only three transitions are allowed: $1 \to 2$, $2 \to 3$, $3 \to 1$, as depicted in Fig. 1.

The master equations that govern the probabilities $p_i(t)$ to find the unit in state i at time t are

$$\begin{aligned} \dot{p}_1 &= g_{31} - (g_{12} + g_{31})\, p_1 - g_{31}p_2 \\ \dot{p}_2 &= -g_{23}p_2 + g_{12}p_1, \end{aligned} \tag{2}$$

where we have eliminated p_3 by using the normalization of probability $p_1 + p_2 + p_3 = 1$.

B. Ensemble of coupled units

The next step is to couple an ensemble of N of these units. Following the prescription proposed in Ref. [9], the transition rates are defined as

$$g_{i,i+1} = g \exp\left[a(U n_{i+1} + V n_{i-1} + W n_i)\right], \tag{3}$$

where

$$n_i(t) = N_i(t)/N \tag{4}$$

is the density of units in state i at time t and $N_i(t)$ is the number of units in this state at this time. Because of the cyclic nature of the units, the state that follows state 3 is state 1, so we implement the mapping $3 + 1 \to 1$ in the subscripts of Eq. (2). Similarly, the state that precedes state 1 is state 3, so we implement the mapping $1 - 1 \to 3$. Moreover, since we can always scale time, we take $g = 1$. Hence, the ensemble dynamics is characterized by the coupling strength a, the weights U, V, and W, and the system size N. Due to the normalization condition $n_1 + n_2 + n_3 = 1$, we can write the transition rates in terms of only two densities, that is,

$$g_{i,i+1} = g_{i,i+1}(n_1, n_2). \tag{5}$$

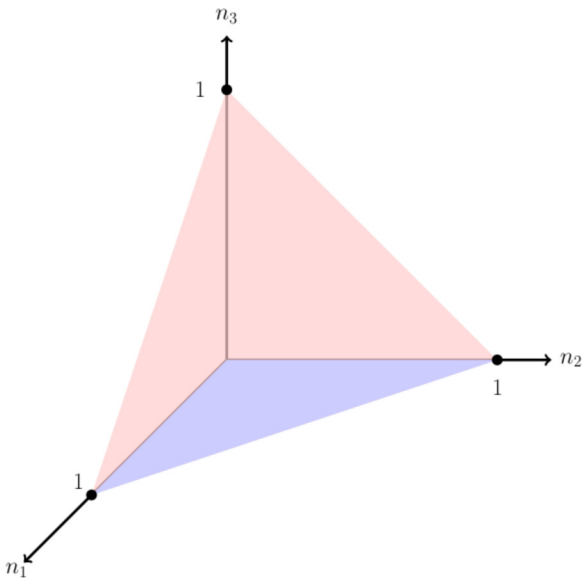

FIG. 2. Two-dimensional triangular phase space (pink) in the three-dimensional world spanned by the three points $n_i = 1$ on which the ensemble of coupled units each of the form of Fig. 1 resides. The triangle in the n_1-n_2 plane (blue) is only there for visual assistance.

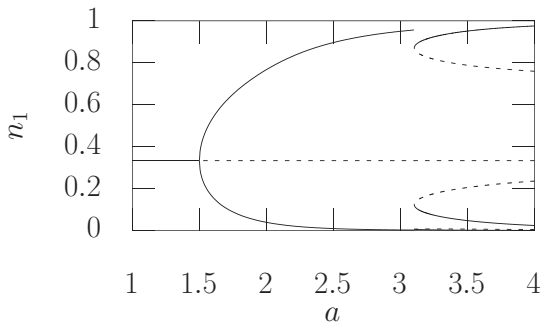

FIG. 3. Bifurcation diagram of the deterministic system, Eq. (7), with the rates given by Eq. (3), for a continuous transition with $(U, V, W) = (1, 0, -1)$. We present the values of n_1 in the steady state as a function of the parameter a. On the left of the figure, a single line represents the symmetric fixed point. After the first bifurcation, the upper and lower curves respectively represent the maximum and minimum values of n_1 in the limit cycle. Hence, all values of n_1 between these lines occur in the limit cycle. After the second bifurcation, the lines represent the fixed points of the asymmetric state. The dashed lines represent the unstable fixed points.

C. Mean-field theory for the coupled ensemble

Ensembles of coupled units ruled by Eq. (3) in the thermodynamic limit $N \to \infty$ were first introduced to study the nonequilibrium transition to synchronization of a locally coupled ensemble with nearest-neighbor interactions [6,7]. In this case a renormalization group type of analysis must be implemented, which leads to a very interesting equilibrium-like critical behavior. That work was followed by mean-field results. We will briefly summarize the known mean-field results in order to provide a context for our new results (we omit results that are not directly related to this work, such as the disordered ensemble reported in Refs. [8,9]).

The main idea behind the mean-field approach is that in the thermodynamic limit one has $n_i(t) \to p_i(t)$, that is,

$$\lim_{N\to\infty} \frac{N_i(t)}{N} = p_i(t). \tag{6}$$

The set of Eq. (2) with the rates Eq. (3) become an autonomous and deterministic dynamical system for these densities [these equations can be written in terms of the $p_i(t)$ or equivalently in terms of the $n_i(t)$]:

$$\begin{aligned} \dot{n}_1 &= g_{31}(n_1, n_2) - [g_{12}(n_1, n_2) + g_{31}(n_1, n_2)]n_1 - g_{31}(n_1, n_2)n_2 \\ \dot{n}_2 &= -g_{23}(n_1, n_2)n_2 + g_{12}(n_1, n_2)n_1. \end{aligned} \tag{7}$$

Note that we are still constrained to $n_1 + n_2 + n_3 = 1$. Therefore, the physically accessible phase space corresponds to the triangle [cf., phase-space triangle (pink) in Fig. 2]

$$(n_1, n_2) \in \{(n_1 > 0) \text{ and } (n_2 > 0) \text{ and } (n_1 + n_2 < 1)\}. \tag{8}$$

Moreover, due to its symmetry, the system always admits the symmetric static solution

$$n_1^* = n_2^* = n_3^* = 1/3, \tag{9}$$

which may be stable or unstable. Instabilities of the symmetric state spontaneously break the symmetry of the ensemble, leading to self-organization. The emergence of self-organized states includes synchronous oscillations, where the entire ensemble oscillates as a single entity, and stationary ordered phases, where one state is more populated than the others. Note that synchronous chaos is not allowed for three-state units; for that we need either four or more states or possibly some type of memory in the transition rates.

1. Continuous transition to synchronization

The first reported form for the rates, Eq. (3), used the weights $(U, V, W) = (1, 0, -1)$. The control parameter is the coupling strength a. Wood *et al.* [6,7] noted that at $a = 3/2$, the system undergoes a supercritical Hopf bifurcation that leads to an oscillatory limit cycle. Later, Assis *et al.* [10] observed that the system undergoes a second transition at $a = 3.102$. At this point, the period of the periodic orbit diverges, giving rise to stationary ordered phases characterized by the higher population of one of the states over the others. More precisely, the system undergoes a saddle-node bifurcation: The periodic orbit disappears and fixed points emerge [24]. There simultaneously appear six fixed points, three of them stable and the other three hyperbolic. The hyperbolic points are connected by heteroclinic orbits.

This set of possible dynamical behaviors is summarized by the cascade of bifurcations that the system undergoes as the coupling strength increases, see Fig. 3. On the left side of the figure, there is a single symmetric fixed point with $n_1 (= n_2 = n_3) = 1/3$. As the coupling strength a grows, the first bifurcation occurs and a periodic orbit appears. As a continues to grow, the limit cycle grows and also becomes slower as it approaches the second bifurcation. Eventually, a reaches the second bifurcation point, the periodic orbits disappear, and six fixed points appear (there is a pair of fixed points very close to $n_1 = 0$ that can not be discerned on the

TABLE I. Continuous transitions $(U, V, W) = (1, 0, -1)$.

Control parameter	Attractors and bifurcations
$a < 3/2$	Symmetric static state
$a = 3/2$	Supercritical Hopf bifurcation
$3/2 < a < 3.102$	Limit cycle
$a = 3.102$	Saddle-node bifurcation of fixed points on a periodic orbit
$a > 3.102$	Three asymmetric static states

TABLE II. Discontinuous transitions $(U, V, W) = (1, -4, 0)$.

Control parameter	Attractors and bifurcations
$a < 2.84$	Symmetric static state
$a = 2.84$	Saddle-node bifurcation to a limit cycle
$2.84 < a < 3$	Bistability between a limit cycle and the symmetric static state
$a = 3$	Subcritical Hopf bifurcation
$a > 3$	Limit cycle

scale of the figure). Alternatively, the bifurcation scenario can be presented in the form of Table I.

2. Discontinuous transition to synchronization

Wood *et al.* [9] fully analyzed another set of weights. For $(U, V, W) = (1, -4, 0)$, for small a the symmetric fixed point is the only asymptotic solution, see Fig. 4. At $a = 2.84$, a saddle-node bifurcation gives rise to a bistability region, for which the symmetric fixed point and a limit cycle are both stable, with an unstable limit cycle in between. This bistable region is clearly displayed in Fig. 4, where for a in the interval [2.84, 3] the limit cycle and fixed point coexist. As a increases further, the unstable limit cycle shrinks and the stable one grows. A subcritical Hopf bifurcation occurs at $a = 3$, when the unstable limit cycle collides with the symmetric fixed point, which becomes unstable. As will become clear later, this bistable region is the more intriguing feature for finite-N systems. Here again, the bifurcation scenario is summarized in Table II.

III. FINITE-N THEORY

A. General framework to treat globally coupled three-state units

We begin this section with a caveat to avoid any misunderstandings. In the introductory material we talked about a single unit that could be in state 1 or 2 or 3, as indicated by the three states in Fig. 1. Now we introduce globally coupled arrays of these units. In these arrays we now talk about the densities of units in these states, n_1, n_2, and n_3. That is, we label the states of the array as 1 and 2 and 3, not to be confused with the states 1, 2, 3 of a single unit. Henceforth we will primarily discuss the density dynamics and phase spaces.

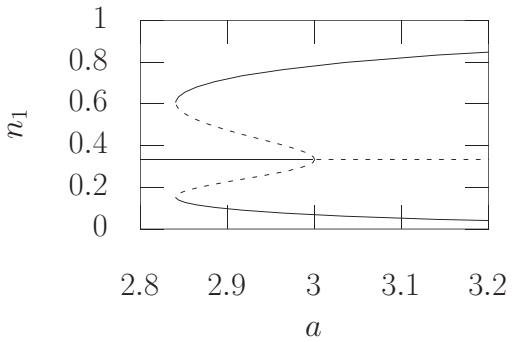

FIG. 4. Bifurcation diagram of the deterministic system, Eq. (7), with the rates given by Eq. (3), for a discontinuous transition with $(U, V, W) = (1, -4, 0)$. We present the values of n_1 in the steady state as a function of the parameter a. In the limit-cycle existence region, the upper and lower curves stand for the maximum and minimum of n_1 for the stable limit cycle, respectively, while the dashed middle curves represent their counterpart for the unstable limit cycle. The horizontal line represents the symmetric fixed point, which is first stable and then at the bifurcation becomes unstable.

We start by analyzing the probability $P(n_1, n_2, t)$ to have the density n_i of units in state i at time t. The master equation that governs this probability can be written as (recall that $n_3 = 1 - n_1 - n_2$)

$$\begin{aligned}\partial_t P(n_1, n_2, t) = & - N_1 g_{12}(n_1, n_2) P(n_1, n_2, t) - N_2 g_{23}(n_1, n_2) \\ & \times P(n_1, n_2, t) - N_3 g_{31}(n_1, n_2) P(n_1, n_2, t) \\ & + (N_1 + 1) g_{12}\left(n_1 + \frac{1}{N}, n_2 - \frac{1}{N}\right) \\ & \times P\left(n_1 + \frac{1}{N}, n_2 - \frac{1}{N}, t\right) \\ & + N_2 g_{23}\left(n_1, n_2 + \frac{1}{N}\right) P\left(n_1, n_2 + \frac{1}{N}, t\right) \\ & + N_3 g_{31}\left(n_1 - \frac{1}{N}, n_2\right) P\left(n_1 - \frac{1}{N}, n_2, t\right).\end{aligned} \tag{10}$$

The first three terms on the right-hand side of this equation (negative terms) correspond to changes in the densities due to the transitions $1 \to 2$, $2 \to 3$, and $3 \to 1$, respectively. The positive contributions can be understood by noting that changes in the densities can only occur in steps of $1/N$ in a system with N units This is the basis of the so-called van Kampen $1/N$ expansion [25,26]. Therefore, the transition from 1 to 2 decreases n_1 and increases n_2 both by $1/N$. Hence, in order for such a transition to decrease the probability density of n_1 and increase the probability density of n_2, the system must have densities $n_1 + 1/N$ and $n_2 - 1/N$. Similarly, for the transition from 2 to 3, n_1 does not change, the density of state 2 must be $n_2 + 1/N$, and that of n_3 must be $n_3 - 1/N$. For the transition from 3 to 1 it is n_2 that does not change, the density of state 3 must be $n_3 + 1/N$, and that of state 1 must be $n_1 - 1/N$. This master equation can be recast as

$$\partial_t P = N \sum_{i=1}^{3} (a_i^+ a_{i+1}^- - 1) T_{i,i+1} P, \tag{11}$$

where, again, we set $3+1 \to 1$ and $T_{i,j} = n_i g_{ij}$. The symbols $a_i^{\pm}$ correspond to ladder operators,

$$a_i^{\pm} f(\dots n_i \dots) = f\left(\dots n_i \pm \frac{1}{N} \dots\right), \tag{12}$$

for any function f. Note that the operations $a_i^{+} a_{i+1}^{-}$ ensure the conservation of the number of elements of the ensemble. Furthermore, we work with the boundary conditions

$$a_i^{-} f(\dots n_i = 0 \dots) = a_i^{+} f(\dots n_i = 1 \dots) = 0, \tag{13}$$

which ensures that the density lies in the interval [0,1].

By expanding the master equation (11) in powers of $1/N$, and neglecting terms $\mathcal{O}(1/N^2)$, we deduce that the probability $P(n_1, n_2, t)$ obeys a Fokker-Planck equation that has the form

$$\partial_t P = \vec{\nabla} \cdot \vec{\Phi}, \tag{14}$$

where the $\vec{\nabla}$ operator and the probability flux $\vec{\Phi}$ are given by

$$\vec{\nabla} = \begin{pmatrix} \partial_{n_1} \\ \partial_{n_2} \end{pmatrix}, \qquad \vec{\Phi} = \begin{pmatrix} \Phi_1 \\ \Phi_2 \end{pmatrix}. \tag{15}$$

After a straightforward calculation, the explicit from of $\vec{\Phi}$ is obtained. It has the form

$$\Phi_i = -A_i P + \frac{1}{2N} \sum_{j=1}^{2} \partial_{n_j} \left(B_{ij} P\right), \tag{16}$$

where the drift vector is given by

$$A = \begin{bmatrix} g_{31}(1 - n_1 - n_2) - g_{12} n_1 \\ g_{12} n_1 - g_{23} n_2 \end{bmatrix} \tag{17}$$

and the diffusion tensor by

$$B = \begin{bmatrix} g_{12} n_1 + g_{31}(1 - n_1 - n_2) & -g_{12} n_1 \\ -g_{12} n_1 & g_{12} n_1 + g_{23} n_2 \end{bmatrix}. \tag{18}$$

Alternatively, one may start from the microscopic dynamics. A simple counting protocol leads to the following equations of motion which describe the microscopic dynamics of N coupled units:

$$\begin{aligned} N_1(t+dt) = N_1(t) &- \sum_{k=1}^{N_1} \theta[g_{12}(n_1, n_2)dt - \zeta_k] \\ &+ \sum_{k=N_1+N_2+1}^{N} \theta[g_{31}(n_1, n_2)dt - \zeta_k], \\ N_2(t+dt) = N_2(t) &- \sum_{k=N_1+1}^{N_1+N_2} \theta[g_{23}(n_1, n_2)dt - \zeta_k] \\ &+ \sum_{k=1}^{N_1} \theta[g_{12}(n_1, n_2)dt - \zeta_k]. \end{aligned} \tag{19}$$

Here $\theta(x)$ is the Heaviside θ function. The set $\{\zeta_k\}_{k=1}^{N}$ is a set of independent random variables uniformly distributed in the interval [0, 1]. Thus, if unit k is in state 1 at time t, then if $g_{12}(n_1, n_2)dt > \zeta_k$, unit k flips from state 1 to state 2. As a consequence N_1 decreases by 1 (first sum in N_1) and N_2 increases by 1 (second sum in N_2). If $g_{12}(n_1, n_2)dt < \zeta_k$, then unit k remains in state 1. If unit k is in state 2 at time t, then if $g_{23}(n_1, n_2)dt > \zeta_k$, unit k flips from state 2 to state 3 and as a consequence N_2 decreases by 1 (first sum in N_2), and N_3 increases by 1, but it is not necessary to show the equation for N_3 because of the conservation condition. If $g_{23}(n_1, n_2)dt < \zeta_k$, then unit k remains in state 2. If unit k is in state 3 at time t, then it moves to state 1 if $g_{31}(n_1, n_2)dt > \zeta_k$, thus increasing N_1 by 1 (second sum in N_1); if $g_{31}(n_1, n_2)dt < \zeta_k$, then the unit remains in state 3. Note that at any given time t, the dynamics of all units in the array are determined by the same rates $g_{ij}(n_1(t), n_2(t))$.

Generalizing the steps presented in detail in Ref. [20] for an ensemble of two-state units to our present case of three-state units, we arrive at the Langevin equations

$$\begin{aligned} \dot{n}_1 &= g_{31}(1 - n_1 - n_2) - g_{12} n_1 \\ &\quad + \sqrt{g_{31}(1 - n_1 - n_2)}\, \frac{\xi_1(t)}{\sqrt{N}} - \sqrt{g_{12} n_1}\, \frac{\xi_2(t)}{\sqrt{N}}, \\ \dot{n}_2 &= g_{12} n_1 - g_{23} n_2 + \sqrt{g_{12} n_1}\, \frac{\xi_2(t)}{\sqrt{N}} - \sqrt{g_{23} n_2}\, \frac{\xi_3(t)}{\sqrt{N}}, \end{aligned} \tag{20}$$

where the $\xi_i(t)$ denote Gaussian distributed independent white noises, with

$$\begin{aligned} \langle \xi_i(t) \rangle &= 0 \\ \langle \xi_i(t) \xi_j(t') \rangle &= \delta_{ij} \delta(t - t'). \end{aligned} \tag{21}$$

These Langevin equations, when interpreted using Itô calculus, lead to the Fokker-Planck equation (14), with the drift vector (17) and the diffusion tensor (18). It is important to note that in the thermodynamic limit $N \to \infty$, the Langevin equations lead to Eq. (7) of the mean-field theory. Moreover, fluctuations decay as $1/\sqrt{N}$, following the standard thermodynamic behavior.

B. Analysis and results

In order to study the stationary probability density $P_0(n_1, n_2)$ one may either perform the direct simulation of the microscopic equations of motion, Eq. (19), or calculate $P_0(n_1, n_2)$ from the Fokker-Planck equation (14) or, equivalently, from the simulation of the Langevin equations. We have ascertained that both paths lead to essentially equivalent results. We shall mostly present only the results from the Fokker-Planck equation, and will point out and explain the slight differences between the stationary solution of the Fokker-Planck equation and the numerical simulations results.

Before discussing our results, we note a clarification about nomenclature. When N is finite there are, strictly speaking, no longer fixed points or limit cycles. There are now fluctuations and so these are no longer strictly defined. However, as N increases, we will show that there are residues of these results but with fluctuations around them that grow smaller in amplitude with increasing N and that disappear entirely when $N \to \infty$. However, we will continue to use these terms for convenience. The "almost" fixed points and limit cycles are now associated with minima (stable) and maxima in the probability distributions, but using the latter terminology is cumbersome, so we revert to the fixed point and limit-cycle loose terminology.

From Eq. (14), the stationary probability $P_0(n_1, n_2)$ must satisfy

$$\vec{\nabla} \cdot \vec{\Phi}(P_0, \vec{\nabla} P_0) = 0. \tag{22}$$

To solve this equation, we applied a finite-element method (FEM) with zero flux boundary conditions at the perimeter of the triangle defined by Eq. (8). More precisely, we used the FreeFem++ partial differential equation solver [27]. In the following sections we discuss our results for finite N separately for the continuous and discontinuous transitions to synchronization. These results are presented in Fig. 5–Fig. 10. Next to each panel there is a bar indicating the color code for the probability density. The top of each bar indicates the high probability color and the bottom of the bar indicates the color used for $P_0(n_1, n_2) = 0$. In between, the colors represent a linear variation of the probability density from zero to the maximum value for each panel.

1. Continuous transition to synchronization

In the mean-field approximation ($N \to \infty$), as the control parameter a is increased the choice of the parameters $(U, V, W) = (1, 0, -1)$ leads to a continuous transition from the symmetric fixed point $n_1^* = n_2^* = n_3^* = 1/3$ to a limit cycle, followed by a second transition to a state with three asymmetric fixed points (cf. Fig. 3). There are of course no finite-number fluctuations in this limit. Figure 5 shows the probability density $P_0(n_1, n_2)$ near the transition from the symmetric fixed point to the limit cycle for different values of N. As expected, smaller systems present larger fluctuations. However, the qualitative behavior is independent of the number of units and approaches the mean-field result as N increases. Similarly, in the synchronized state, a limit cycle is more evident for larger systems (see Fig. 6). In both cases, the results from direct simulations (not shown) and the Fokker-Planck equation are equivalent.

In the frozen state, however, the results from a single long simulation and the Fokker-Planck equation differ. While the stationary solution of the Fokker-Planck equation shows the three symmetric fixed points, the time evolution of the microscopic equations of motion leads the system to one of the fixed points, where it stays for the remainder of the simulation. Obviously, the choice among the three fixed points (starting from the symmetric state) is equally probable. To recover the results of the Fokker-Planck equation, one would need to run several simulations and average the probability distributions because there is an ergodicity breaking in each single simulation. We abstain from showing the density plots because they show just a small red blur near the fixed points over a uniform background.

In summary, for the continuous transition case, the fluctuations due to the finite number of units bring almost no new feature to the dynamical evolution of the system. Probably, the single qualitative difference between the mean-field approximation ($N \to \infty$) and the finite-N case appears in the frozen state. While in the mean-field approximation the initial condition completely determines to which of the fixed points the system goes, in the finite-N case fluctuations play a role

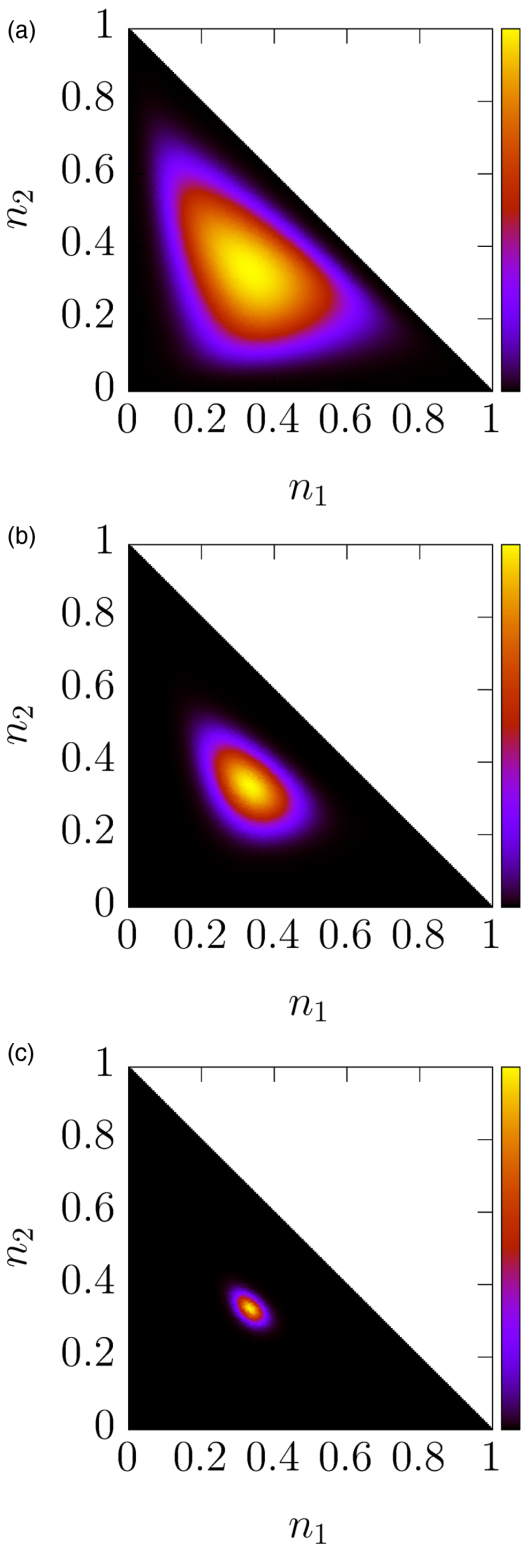

FIG. 5. Density plots for the stationary solution of the Fokker-Planck equation (14) for $(U, V, W) = (1, 0, -1)$ and $a = 1.4$ (below the bifurcation value $a = 1.5$ to the limit cycle in the mean-field approximation). From top to bottom, (a) $N = 100$, (b) 500, and (c) 5000. When $N = 5000$ the symmetric fixed point is most clearly evident. See text for description of color bar to the right of each panel in this and subsequent figures.

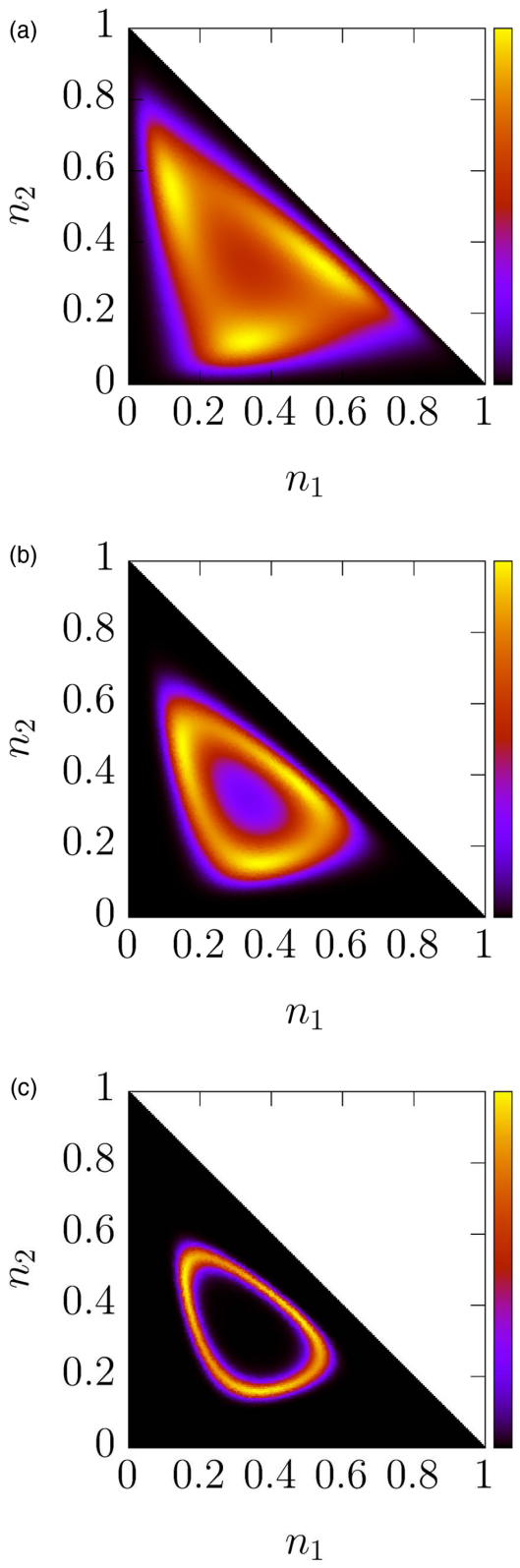

FIG. 6. Density plots for the stationary solution of the Fokker-Planck equation (14) for $(U, V, W) = (1, 0, -1)$ and $a = 1.6$ (above the bifurcation point). From top to bottom, (a) $N = 100$, (b) 500, and (c) 5000. When $N = 5000$ the limit cycle is most clearly evident.

and the same initial conditions may lead to different outcomes (particularly for smaller systems).

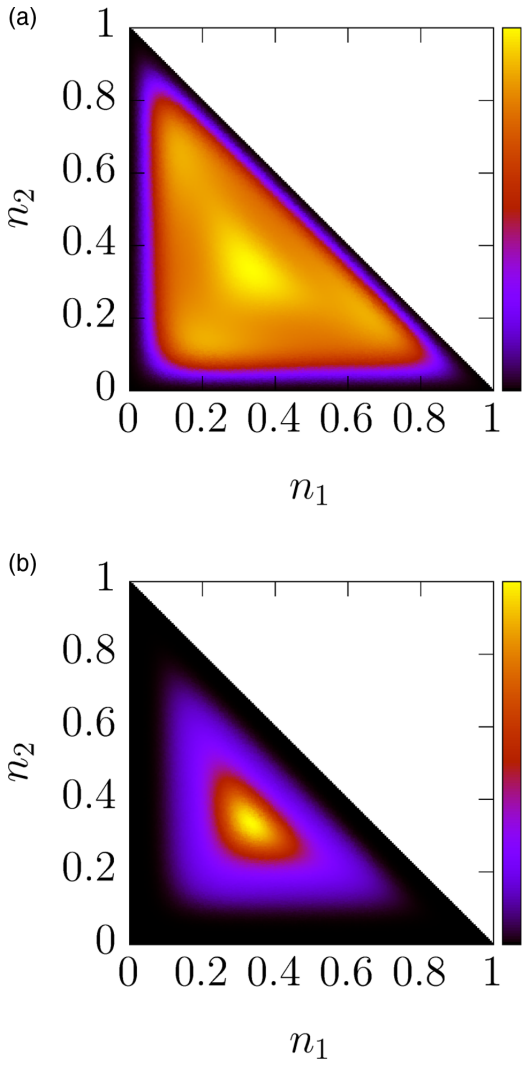

FIG. 7. Density plots for the stationary solution of the Fokker-Planck equation (14), for $(U, V, W) = (1, -4, 0)$. Here $a = 2.8$ and the number of units is $N = 100$ (a) and $N = 500$ (b). For reference, the bifurcation point for infinite systems occurs at $a = 2.84$.

2. Discontinuous transition to synchronization

A coexistence region in the mean-field bifurcation diagram, such as occurs with the choice $(U, V, W) = (1, -4, 0)$, cf. Fig. 4, makes the finite-N behavior more intriguing. While deep in the fixed-point-only stability region or in the limit-cycle-only stability region, one or the other regime is clear even for small systems. As we approach the bifurcation, hints of the coexistence already appear for small values of N away from the critical mean-field value of the control parameter. For instance, in Figs. 7 and 8 we show the density plots of the probability distribution for two values of the control parameter a below the critical value—one far below the bifurcation point $a = 2.84$ ($a = 2.8$, Fig. 7) and the other nearer to it ($a = 2.835$, Fig. 8)—and two system sizes: $N = 100$ (top panels) and $N = 500$ (bottom panels). Clearly, for the larger systems (bottom panels) the symmetric fixed point is the preferred state, with fluctuations being seen around it. For the smaller systems, the symmetric fixed point is the preferred state away from the bifurcation point (top panel

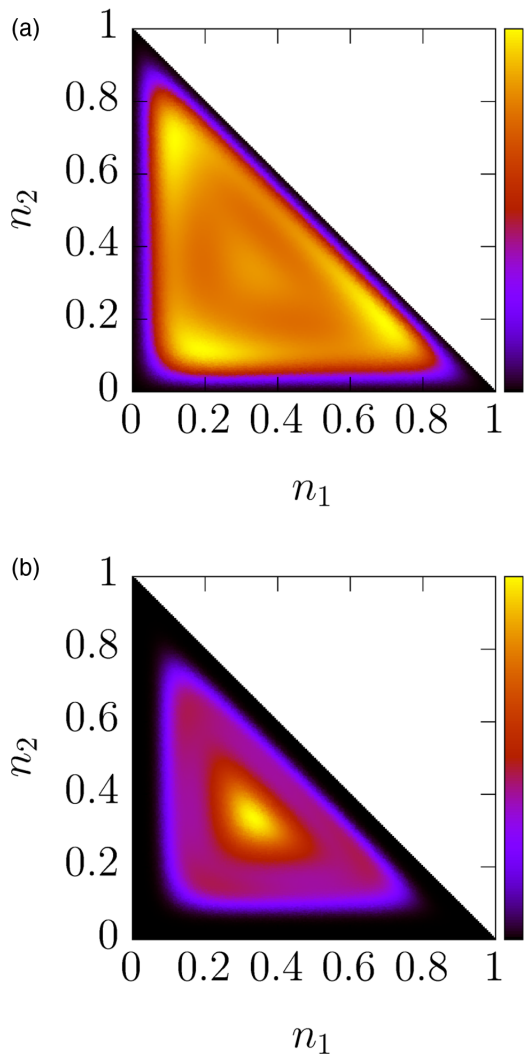

FIG. 8. Density plots for the stationary solution of the Fokker-Planck equation (14) for $(U, V, W) = (1, -4, 0)$. Here $a = 2.835$ and the number of units is $N = 100$ (a) and $N = 500$ (b). For reference, the bifurcation point for infinite systems occurs at $a = 2.84$.

in Fig. 7). However, close to the bifurcation point, for the smaller system one may argue that there is a coexistence, and the limit cycle may even be the dominant state (top panel in Fig. 8).

To illustrate the behavior of the system in the coexistence region in more detail, we show Figs. 9 and 10. For small systems one can see the coexistence of the fixed point and the limit cycle (see Figs. 9 and 10, top panels). As the system size increases, the coexistence fades and either the fixed point (Fig. 9) or the limit cycle (Fig. 10) dominates. In all cases, the results of the numerical simulations (results not shown) and the steady state of the Fokker-Planck equation are indistinguishable. Furthermore, for the $a = 2.87$ case, we calculate the steady state for an even larger population ($N = 20\,000$), as shown in the bottom panel of Fig. 10. We can clearly see a reinforcement of the breakdown of the bistability.

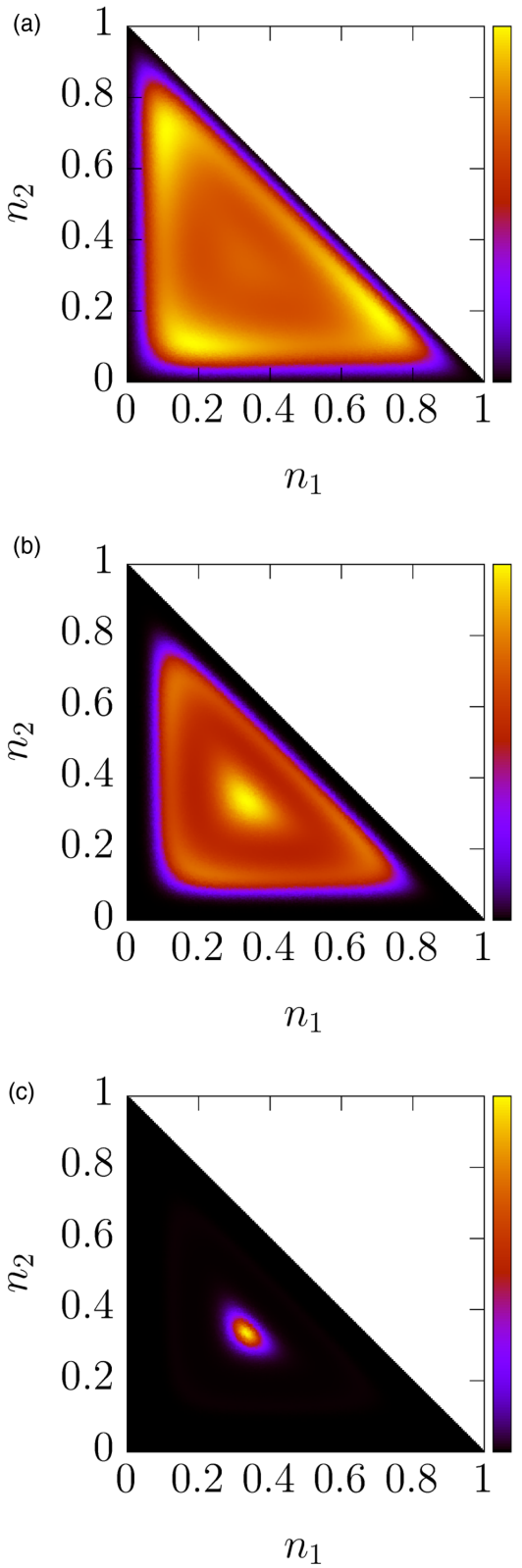

FIG. 9. Density plots for the stationary solution of the Fokker-Planck equation (14) for $(U, V, W) = (1, -4, 0)$ and $a = 2.85$. The critical value for infinite systems is $a = 2.84$. From top to bottom, (a) $N = 100$, (b) 500, and (c) 5000.

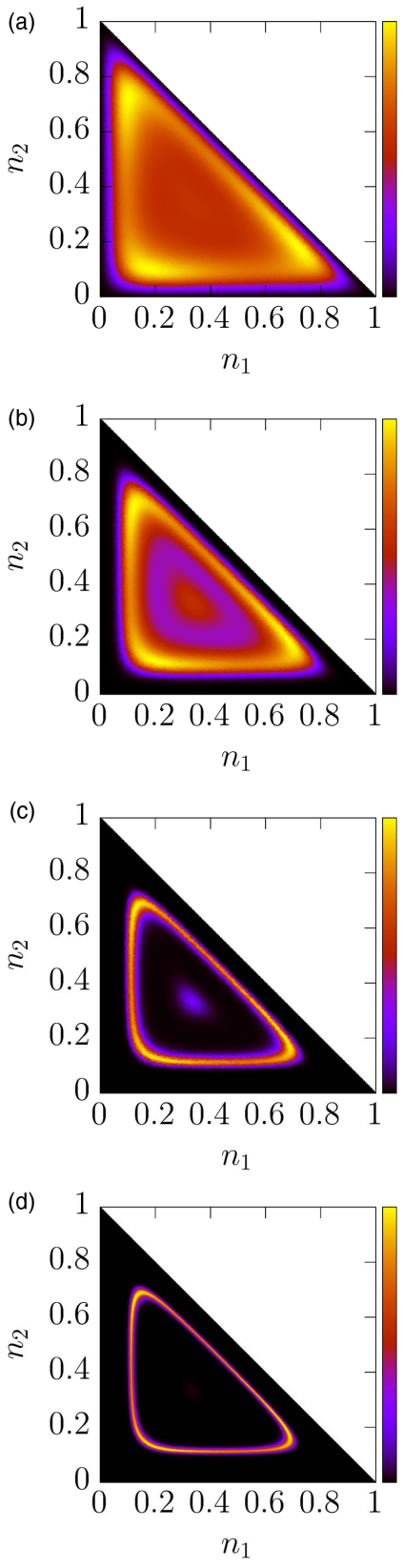

FIG. 10. Density plots for the stationary solution of the Fokker-Planck equation (14) for $(U, V, W) = (1, -4, 0)$ and $a = 2.87$. The critical value for infinite systems is $a = 2.84$. From top to bottom, (a) $N = 100$, (b) 500, (c) 5000, and (d) 20 000.

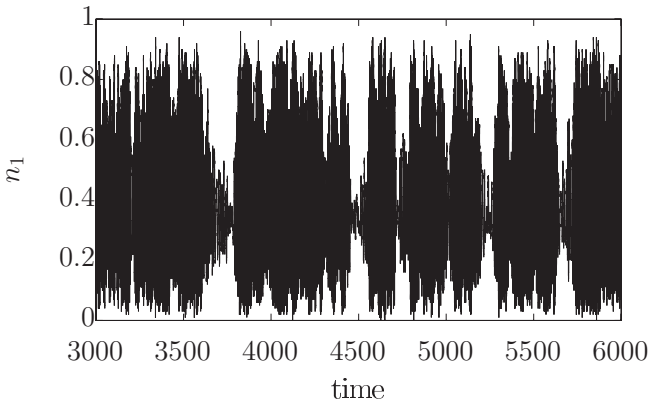

FIG. 11. Time evolution of the density $n_1(t)$ for $(U, V, W) = (1, -4, 0)$, $a = 2.85$, and $N = 100$. The critical value for infinite systems is $a = 2.84$. The data were obtained via the direct simulation of Eq. (19).

It is worth noting that despite the relation between the maxima of the stationary state probability distribution for finite-N systems and the stable solutions in infinite systems, there is a fundamental distinction that must be recalled again and again. As noted earlier, while for infinite systems the dynamics is deterministic, for finite N the dynamics is stochastic. Therefore, for infinite systems the initial condition completely determines the fate of the evolution of the system. In particular, in the coexistence region the system will end up in a stable limit cycle if the initial condition lies outside of the unstable limit cycle, whereas it goes to the fixed point otherwise. For finite-N systems, especially for small systems, the initial conditions are almost irrelevant. For instance, in Fig. 11 we show the time evolution of the density $n_1(t)$ for a small system ($N = 100$) in the coexistence region. The initial condition was near the symmetric state ($n_1 = n_2 = 1/3$), but the evolution of the system rapidly goes into a stationary state where the periodic orbit (regions of large variations in the values of n_1) coexist with the symmetric state. For large systems the initial conditions are also negligible. That is, after a transient, the system goes to one or the other stable state (in the language of the deterministic system) and stays there a longer and longer time as N increases. Which one of the stable states the system evolves to, contrary to the infinite system case, is not determined by the initial condition but by the control parameter alone. Between the small and large N scenarios, one of the maxima of the probability distribution (corresponding to the fixed point or the limit cycle) grows and the other diminishes as N increases. This behavior is reminiscent of the one we observed previously in two-state systems [20,21] showing the difference of which limit is taken first, $t \to \infty$ (finite-N approach) or $N \to \infty$ (mean-field approach). In the two-state case, we were able to write a formal solution to the Fokker-Planck equation in terms of an effective potential. It turns out that as N increases the depth of one minimum of the effective potential becomes increasingly deeper than the other, that is, one of the fixed points becomes much more probable than the other. It is worth mentioning that, particularly in the three-state case, the

duration of the transient increases with N. Therefore, short simulations of the master equation or the Langevin equation may seem to indicate the persistence of the bistability (we discuss this question in more detail in Appendix B). This transient behavior is avoided by calculating the steady state of the Fokker-Planck equation. It is worth mentioning that even this method has its caveats. For very large systems the probability distribution becomes extremely sharp and a finer mesh is necessary, which increases the computer time. We tested systems with up to $N = 50\,000$ units and confirmed that the trends discussed above persist.

3. Order parameter

In the previous sections we extensively discussed the qualitative dependence of the steady state on the system size. Next we turn to quantitative measures in a more systematic characterization of the steady-state distribution. We start by analyzing the order parameter of the system. In fact, two order parameters have been used in the literature to study this model in the mean-field limit. First, there is a version of the Kuramoto order parameter r adapted to this system, for which one may interpret the three discrete states as coarse-grained phases of an oscillator, that is,

$$\{1, 2, 3\} \to \{0, 2\pi/3, 4\pi/3\}. \tag{23}$$

Then, denoting the phase of the kth unit in the ensemble by ϕ_k, the Kuramoto order parameter becomes

$$\begin{aligned} r &= \left| \frac{1}{N} \sum_{k=1}^{N} \exp(i\phi_k) \right| \\ &= |n_1 + n_2 \exp(i2\pi/3) + (1 - n_1 - n_2) \exp(i4\pi/3)|. \end{aligned} \tag{24}$$

This order parameter has been used since the early studies of this model [6,7]. It successfully detects the transition from the symmetric fixed point to the limit cycle, but it is meaningless in the transition from the limit cycle to the three asymmetric fixed points.

The second order parameter was proposed by Assis *et al.* [10] in order to characterize the second transition for $(U, V, W) = (1, 0, -1)$. It is defined as

$$\begin{aligned} \Psi &= \left| \frac{1}{N} \sum_{k=1}^{N} \exp(i\phi_k) g_{k,k+1} \right| \\ &= |n_1 g_{12} + n_2 \exp(i2\pi/3) g_{23} \\ &\quad + (1 - n_1 - n_2) \exp(i4\pi/3) g_{31}|. \end{aligned} \tag{25}$$

with g_{ij} as defined in Eq. (3). This order parameter vanishes as we approach not only the symmetric fixed point, as does Kuramoto's order parameter Eq. (24), but also the three asymmetric ones.

We have studied both order parameters, (24) and (25). More precisely, their expected values at the nonequilibrium stationary state are

$$\langle r \rangle = \int_{\Omega} r\, P_0(n_1, n_2)\, dn_1 dn_2, \tag{26}$$

$$\langle \Psi \rangle = \int_{\Omega} \Psi\, P_0(n_1, n_2)\, dn_1 dn_2, \tag{27}$$

where Ω denotes the triangle defined by Eq. (8) and $\langle\rangle$ denotes a steady-state average. However, since $\langle\Psi\rangle$ captures all the information that Kuramoto's order parameter does, we discuss only the results for $\langle\Psi\rangle$.

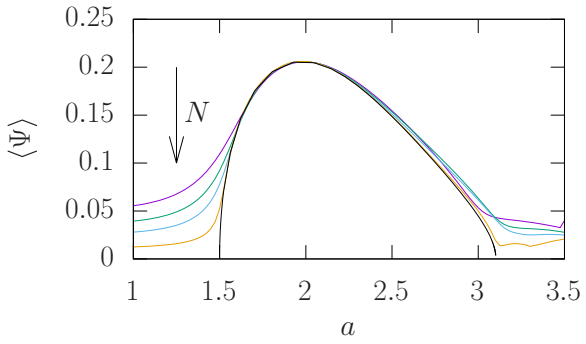

FIG. 12. Steady-state averages of the order parameters for the continuous transition case $(U, V, W) = (1, 0, -1)$ for various values of N (250, 500, 1000, and 5000) and for the mean-field case ($N \to \infty$).

Figure 12 displays our computations for the steady-state averages of the order parameter $\langle\Psi\rangle$, for $(U, V, W) = (1, 0, -1)$. As N increases, the order parameter for finite systems approaches the mean-field result, as expected. Moreover, the finite-size systems show ordering before the transition point predicted by the mean-field theory. That is, the fluctuations activate a *precursor* of the synchronous phase (that can also be seen in the density plots). Similar phenomena have been reported in the context of pattern formation systems, where fluctuations give rise to a preferential wavelength even below the Turing instability critical point. This idea can also be applied for a frequency instead of a wavelength (time instead of space) [28–32].

Figure 13 displays the same steady-state averages of the order parameter $\langle\Psi\rangle$ for the choice $(U, V, W) = (1, -4, 0)$.

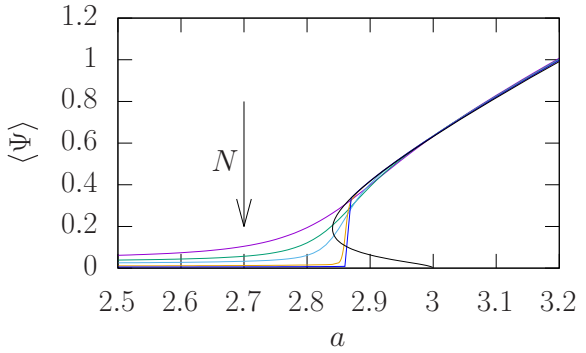

FIG. 13. Steady-state averages of the order parameters for the discontinuous transition case $(U, V, W) = (1, -4, 0)$ for various values of N (250, 500, 1000, 5000, and 20 000) and for the mean-field case ($N \to \infty$).

Here, in addition to the precursor, we notice that the order parameter for finite systems does not approach the mean-field result as N grows—note that in the mean-field limit the order parameter is not uniquely defined in the coexistence region (it has one value for each steady-state solution, namely, the stable limit cycle, the unstable limit cycle and the fixed point, for which it is zero). That is, the bistable behavior predicted by the mean-field approach is absent for finite-N. When the limit $N \to \infty$ is taken before the limit $t \to \infty$, ergodicity is lost. In other words, the steady state predicted by Eq. (7) depends on the initial condition because the system does not explore the entire accessible phase space [i.e., the triangle defined by Eq. (8)]. In contrast, the Fokker-Planck steady state only takes account of the limit $t \to \infty$, becoming initial condition independent. Moreover, further increasing the value of N, the transition to synchrony becomes first order (see the Appendix A). In fact, as we increase N the order parameter curve becomes steeper, indicating that a jump (discontinuity) occurs for $N \to \infty$. Actually, this is consistent with the qualitative behavior observed in the density plots of Figs. 9 and 10, for which, inside the coexistence region, for large systems either the symmetric fixed point or the limit cycle prevails.

4. Angular velocity in the steady state

In order to further characterize the dynamics of the steady state, we study the angular velocity. To define it, let us go back to the original three dimensional phase space (n_1, n_2, n_3), with the constraint $n_1 + n_2 + n_3 = 1$. Then the accessible phase space corresponds to the equilateral triangle with vertices $(1, 0, 0)$, $(0, 1, 0)$, and $(0, 0, 1)$. The barycenter of the triangle corresponds to the symmetric solution $n_1 = n_2 = n_3 = 1/3$. Consequently, the angular velocity of a point (n_1, n_2, n_3) can be defined as

$$\omega(n_1, n_2, n_3) = \left| \frac{\vec{r} \times \vec{v}}{r^2} \right|, \tag{28}$$

where $\vec{r}$ is the position of the point in the reference frame of the barycenter of the triangle, and $\vec{v}$ is the velocity of the point. To estimate the velocity, we have used its mean-field value

$$\vec{v} = \begin{pmatrix} \dot{n}_1 \\ \dot{n}_2 \\ \dot{n}_3 \end{pmatrix} = \begin{pmatrix} g_{31} n_3 - g_{12} n_1 \\ g_{12} n_1 - g_{23} n_2 \\ g_{23} n_2 - g_{31} n_3 \end{pmatrix},$$

and computed the steady-state mean value of the angular velocity

$$\langle \omega \rangle = \int_\Omega \omega(n_1, n_2, 1 - n_1 - n_2)\, P_0(n_1, n_2)\, dn_1 dn_2.$$

Figure 14 displays our results for the mean angular velocity in the steady state for $(U, V, W) = (1, 0, -1)$. As we see, below the critical point ($a = 1.5$) the angular velocity tends to a constant value $\langle \omega \rangle \cong 0.87$. It is, again, a consequence of the precursor of the synchronous state. In fact, linearizing Eq. (7) around the symmetric fixed point $n_1 = n_2 = 1/3$, one obtains

$$\delta \dot{\vec{n}} = \mathcal{D} \delta \vec{n},$$

where $\delta \vec{n} = (n_1 - 1/3, n_2 - 1/3)$ and $\mathcal{D}$ is the Jacobian matrix of the nonlinear forces that appears in Eq. (7), evaluated

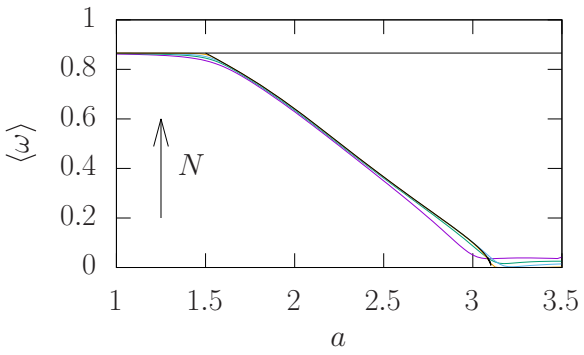

FIG. 14. Mean angular velocity in the steady state, as a function of the coupling strength a, for $(U, V, W) = (1, 0, -1)$ and various values of N (250, 500, 1000, and 5000). The dashed line is the theoretical prediction $\omega_L = \sqrt{3}/2$ for $N \to \infty$. The solid black line is the mean-field deterministic result.

at the fixed point $n_1 = n_2 = 1/3$. The eigenvalues of $\mathcal{D}$ are

$$D_\pm = (a - 3/2) \pm i \frac{\sqrt{3}}{2}.$$

Therefore, below criticality ($a < 1.5$), small perturbations to the angular velocity of a symmetric fixed point behaves as an underdamped oscillator. The frequency of oscillations, which is predicted by this linear analysis, is $\omega_L = \sqrt{3}/2 \cong 0.866$ (represented by the dashed line in Fig. 14), which coincides with the mean value angular velocity that is estimated from the numerical computation of the Fokker-Planck equation steady state. Hence, for the finite-size systems the fluctuations respect the natural tendency of the units to oscillate in unison, as a precursor of synchrony. Above criticality ($a > 1.5$), the oscillation frequency predicted by this linear analysis only works very near to the critical point. Then, the frequency starts to decrease (almost linearly with the control parameter), vanishing as the infinite-period bifurcation, predicted by the mean-field theory (with the secondary critical point taking place at $a = 3.102$), which leads to the formation of the three asymmetric fixed points.

Figure 15 displays our computations of the mean value angular velocity for $(U, V, W) = (1, -4, 0)$. Here we have a similar scenario, that is, small perturbations to the nonsynchronous state behaves as an underdamped oscillator before the transition from the fixed point to the limit cycle. In this case, however, the frequency of oscillation that is predicted by the linear analysis depends on the control parameter,

$$\omega_L(a) = \frac{\sqrt{3}}{2} e^{-a} (1 + 3a).$$

From the starting point of Fig. 15 to the transition to the periodic behavior, the angular velocity decreases monotonically, approaching the predicted value given by Eq. (28), dashed line in the figure, as N increases. The tendency of the angular velocities computed from the steady state of the Fokker-Planck equation steady state to be larger for smaller values of N can be attributed to the presence of other oscillation frequencies, which is related to the angular velocity of the limit cycles that appear by saddle-node bifurcation at $a = 2.8$. Even for $a < 2.8$, the ghost of these limit cycles may influence the average

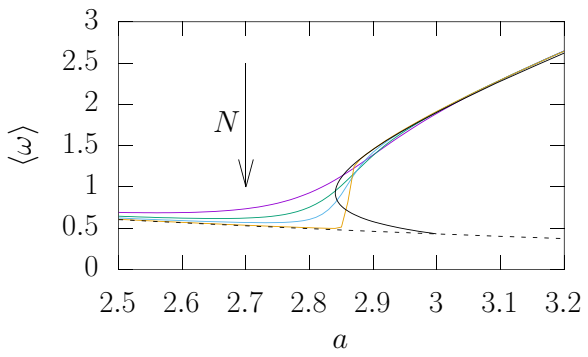

FIG. 15. Mean angular velocity in the steady state as a function of the coupling strength a, for $(U, V, W) = (1, -4, 0)$ and various values of N (250, 500, 1000, and 5000). The dashed line is the theoretical prediction $\omega_L = (\sqrt{3}/2)e^{-a}(1 + 3a)$ for $N \to \infty$. The solid black line is the mean-field deterministic result. We can see a coexistence of a stable and an unstable limit cycle for $2.84 < a < 3$ that is consistent with the subcritical Hopf bifurcation described earlier.

angular velocity of the fluctuating system. This is, of course, a nonlinear effect that requires larger fluctuations (i.e., small N) to manifest. In fact, as N increases, the average angular velocity get closer and closer to the values of $\omega_L(a)$, up to the jump to higher values that are dictated by the stable limit cycle. This can be seen neatly in the curve that corresponds to $N = 5000$ in Fig. 15, showing again a signature of a first-order (discontinuous) transition to synchrony when the limit $t \to \infty$ is taken before $N \to \infty$.

IV. SUMMARY AND CONCLUDING REMARKS

In this report we have analyzed arrays of a finite number N of interacting three-state units to explore the synchronization properties of the array. There are two sources of randomness in our model: One is the fact that the transitions of each unit from one state to another are described by a rate, and the other is due to the finite number of units. It is the latter that we have examined in this work. The three-state units interact due to a prescription [see Eq. (3)] already reported in the literature [6–10]. We described the system using a Fokker-Planck equation and numerically computed (using finite-element methods) the steady state of the array. Therefore, in contrast with mean-field theory that first implements the limit $N \to \infty$ and then $t \to \infty$, the steady-state distribution that is obtained from the Fokker-Planck equation only takes the limit $t \to \infty$, keeping N finite.

In particular, we focused on two cases that, at the level of the mean-field description, offer very rich dynamics as a function of the control parameter a. In the first case, the mean-field description presents a supercritical Hopf bifurcation for $a = 3/2$ that gives rise to a limit cycle and a saddle-node bifurcation for which the limit cycle disappears. In this case, the consequences of having a finite number of units are limited. Basically, the finite number introduces fluctuations that can be seen around the stable solutions of the mean-field description. As N increases, these fluctuations fade away and the system approaches the mean-field solutions, regardless of the value of the control parameter.

In the second case, for which the mean-field description predicts a coexistence region between the symmetric fixed points and a limit cycle, the effect of the finite number of units is much more prominent. While for small N the fluctuations are so large that coexistence seems to be present, when the number of units increases, instead of the reinforcement of the coexistence, the system chooses one or the other mean-field stable solution depending only on the value of the control parameter. We carefully analyzed this transition with the help of the order parameter Ψ and the angular velocity ω, showing that a first-order transition takes place in the finite-N case. Therefore, the order in which we take the limits of time t and number of units N to go to infinity can strongly impact the behavior of the steady-state solutions all over the bistability region.

In our earlier work [20,21], we considered many of these questions for arrays of two-state units rather than three-state ones. This means that our earlier work takes place in one dimension while the current work considers two dimensions. In the three-state case when there is a second-order transition there is no coexistence and so there is only one attractor. In the two-state case there is coexistence of two stable fixed points but there are no limit cycles. In both of these situations the order of the limits $N \to \infty$ and $t \to \infty$ does not matter. However, in the case of the first-order transition of the three-state arrays, there is coexistence of two attractors, a stable fixed point and a limit cycle when $N \to \infty$. When N is finite, however, the fluctuations destroy the coexistence and one of the two states is chosen. Here the order of the limits does matter. Here our main focus has been the two-dimensional situation where limit cycles become possible.

ACKNOWLEDGMENTS

A.R. acknowledges the financial support of CNPq (Grant No. 308344/2018-9). I.P. acknowledges the financial support of FACEPE (Grant No. BFP-0146-1.05/18). D.E. and J.C. thank funding from Fondecyt-Chile (Grant No. 1170669).

APPENDIX A: BINDER CUMULANT

To determine the order of the transitions as N increases, we turn to the Binder cumulant or fourth-order cumulant,

$$U_L = 1 - \langle r^4 \rangle / 3 \langle r^2 \rangle^2, \tag{A1}$$

where r is the order parameter defined in Eq. (24). For second-order transitions, the Binder cumulant for systems of different sizes all cross at a single point that is the critical temperature (here the critical value of the parameter a) for an infinite system. For first-order transitions, Binder *et al.* [33,34] noticed that such cumulant still crosses near the critical value, but the more important feature is that now it presents a minimum (the larger the system the deeper is the minimum). For the continuous transition ($U = 1$, $V = 0$, $W = -1$), we have that curves for different system sizes cross near $a_c = 1.5$ (see Fig. 16, upper panel) and we do not see any minimum, confirming a continuous phase transition. For the discontinuous case ($U = 1$, $V = -4$, $W = 0$) the Binder cumulant

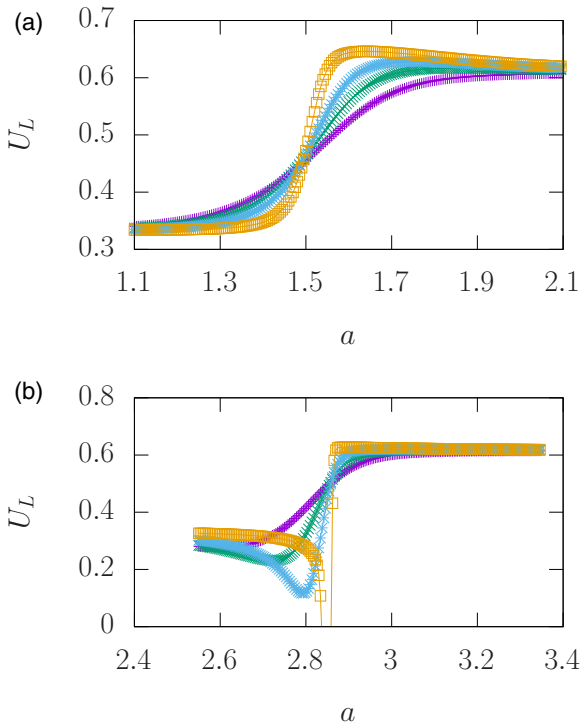

FIG. 16. Binder cumulant as a function of the coupling strength a for various values of N (250, 500, 1000, and 5000). In (a) (continuous transition) we have $(U, V, W) = (1, 0, -1)$, while in (b) (discontinuous transition) $(U, V, W) = (1, -4, 0)$.

curves (see Fig. 16, bottom panel) cross near $a_c = 2.84$ and do present a minimum, confirming that we do have a first-order transition.

APPENDIX B: NUMERICAL SIMULATIONS

In addition to the numerical solution of the Fokker-Planck equation discussed above, we also performed the direct simulation of the Langevin equation Eq. (20). Starting the simulation with all states with the same density $(n_1 = n_2 = n_3 = 1/3)$ we let the system evolve for a long time up to $t = 6 \times 10^7$. Then we calculated a time average of the probability distribution $P(n_1, n_2)$ during a time interval of 10^4 units of time. The results of the simulations were mostly indistinguishable from the results of the solution of the Fokker-Planck equation. In Fig. 17, we show the results of the numerical simulations for $a = 2.87$ and $N = 20\,000$. The comparison of this figure with the bottom panel of Fig. 10 illustrates the equivalence of the two methods.

It should be noted that for large N the relaxation time of the system increases and the results can be misleading. For instance, for $N = 20\,000$, if we use the same initial conditions as before $(n_1 = n_2 = n_3 = 1/3)$ and wait, for instance, for 10^6 units of time before making the measurements, the density plot will be characterized by a single bright spot around the fixed point. On the other hand, using an initial condition outside of the limit cycle we get the limit cycle. Therefore, one may think that the bistability is still present. However, this result occur because the transient was not reached before the

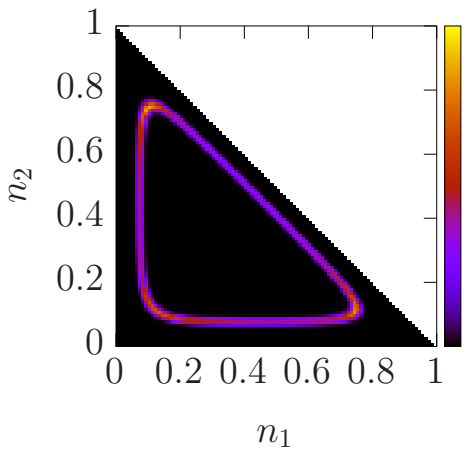

FIG. 17. Density plot for the probability density $P(n_1, n_2)$ obtained from the direct simulation of the Langevin equation Eq. (20), for $(U, V, W) = (1, -4, 0)$, $a = 2.87$, and $N = 20\,000$.

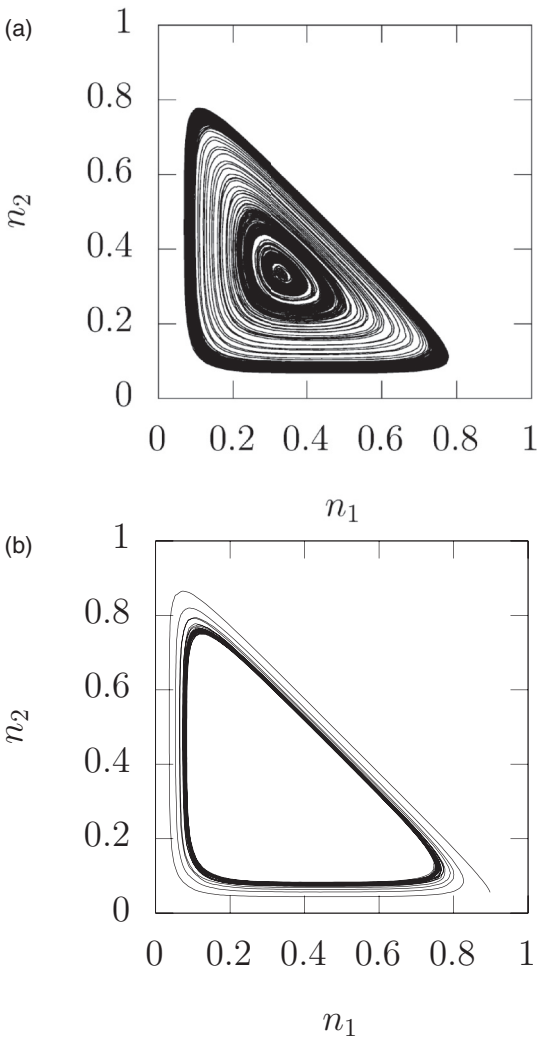

FIG. 18. Orbits of the simulation of the Langevin equation (20) for $(U, V, W) = (1, -4, 0)$, $a = 2.87$, and $N = 20\,000$. In (a) the initial condition was near the symmetric state $n_1 = n_2 = n_3 = 1/3$, while in (b) we started with $n_1 = 0.9$, $n_2 = 0.05$, and $n_3 = 0.05$.

measurements. As shown in Fig. 17, after the long transient we end up in the limit cycle even if we start at the fixed point. Actually, to be sure that the reverse jump (from the limit cycle to the fixed point) does not occur, we ran the simulation up to 10^9 units of time and the system never left the surroundings of the limit cycle.

We end this Appendix presenting the orbits of the simulations of the Langevin equations for two different initial conditions. In the top panel of Fig. 18, the initial conditions were chosen close to the fixed point and we can see the orbit describing an outward spiral in the direction of the limit cycle. The long transient is illustrated by the number of turns that the orbit describes before reaching the neighborhood of the limit cycle. In the bottom panel, the initial conditions were chosen outside the limit cycle and we can see a fast spiral toward the limit cycle.

[1] A. T. Winfree, J. Theor. Biol. **16**, 15 (1967).
[2] Y. Kuramoto, *International Symposium on Mathematical Problems in Theoretical Physics*, Springer Lecture Notes in Physics (Springer, Berlin, 1975).
[3] S. H. Strogatz, Physica D **143**, 1 (2000).
[4] J. A. Acebrón, L. L. Bonilla, C. J. Perez Vicente, F. Ritort and R. Spigler, Rev. Mod. Phys. **77**, 137 (2005).
[5] A. Motter and R. Albert, Phys. Today **65**, 43 (2012).
[6] K. Wood, C. Van den Broeck, R. Kawai, and K. Lindenberg, Phys. Rev. Lett. **96**, 145701 (2006).
[7] K. Wood, C. Van den Broeck, R. Kawai, and K. Lindenberg, Phys. Rev. E **74**, 031113 (2006).
[8] K. Wood, C. Van den Broeck, R. Kawai, and K. Lindenberg, Phys. Rev. E **75**, 041107 (2007).
[9] K. Wood, C. Van den Broeck, R. Kawai, and K. Lindenberg, Phys. Rev. E **76**, 041132 (2007).
[10] V. R. V. Assis, M. Copelli, and R. Dickman, J. Stat. Mech.: Theory Exp. (2011) P09023.
[11] V. R. V. Assis and M. Copelli, Physica A **391**, 1900 (2012).
[12] T. Prager, B. Naundorf, and L. Schimansky-Geier, Physica A **325**, 176 (2003).
[13] T. Prager, M. Falcke, L. Schimansky-Geier, and M. A. Zaks, Phys. Rev. E **76**, 011118 (2007).
[14] N. Kouvaris, F. Müller, and L. Schimansky-Geier, Phys. Rev. E **82**, 061124 (2010).
[15] D. Huber and L. S. Tsimring, Phys. Rev. E **71**, 036150 (2005).
[16] B. Fernandez and L. S. Tsimring, Phys. Rev. Lett. **100**, 165705 (2008).
[17] T. Danino, O. Mondragón-Palomino, L. Tsimring, and J. Hasty, Nature **463**, 326 (2010).
[18] D. Escaff, U. Harbola, and K. Lindenberg, Phys. Rev. E **86**, 011131 (2012).
[19] D. Escaff and K. Lindenberg, Eur. Phys. J.: Spec. Top. **223**, 155 (2014).
[20] I. L. D. Pinto, D. Escaff, U. Harbola, A. Rosas, and K. Lindenberg, Phys. Rev. E **89**, 052143 (2014).
[21] A. Rosas, D. Escaff, I. L. D. Pinto, and K. Lindenberg, J. Phys. A **49**, 095001 (2016).
[22] H. Hong, H. Chaté, L.-H. Tang, and H. Park, Phys. Rev. E **92**, 022122 (2015).
[23] D. Pazó, Phys. Rev. E **72**, 046211 (2005).
[24] J. P. Keener, SIAM J. Appl. Math. **41**, 127 (1981).
[25] N. G. van Kampen, *Stochastic Processes in Physics and Chemistry*, 3rd ed. (Elsevier, Amsterdam, 2007).
[26] C. W. Gardiner, *Handbook of Stochastic Methods* (Springer-Verlag, Berlin, 1983).
[27] F. Hecht, J. Numer. Math. **20**, 251 (2012).
[28] C. Jeffries and K. Wiesenfeld, Phys. Rev. A **31**, 1077 (1985).
[29] M. Wu, G. Ahlers, and D. S. Cannell, Phys. Rev. Lett. **75**, 1743 (1995).
[30] G. Agez, C. Szwaj, E. Louvergneaux, and P. Glorieux, Phys. Rev. A **66**, 063805 (2002).
[31] T. Butler and N. Goldenfeld, Phys. Rev. E **80**, 030902(R) (2009).
[32] T. Biancalani, D. Fanelli and F. Di Patti, Phys. Rev. E **81**, 046215 (2010).
[33] K. Binder, Z. Phys. B: Condens. Matter **43**, 119 (1981).
[34] K. Binder, Phys. Rev. Lett. **47**, 693 (1981).